

ABSTRACT

VEMULA, DHEERAJ. Design and Analysis of an Orderly Recruitment Valve for Bio-inspired Fluidic Artificial Muscles. (Under the direction of Dr. Matthew Bryant).

The objective of this research is to design and analyze a novel hydraulic orderly recruitment valve (ORV) for actuation of fluidic artificial muscle (FAM) systems. Recently artificial muscles are gaining popularity due to their increased efficiency by employing strategies such as variable recruitment (VR). VR employs selective recruitment of parallel muscle actuators depending on the load, akin to the motor recruitment of mammalian muscles. However, existing VR systems have high complexity like the active VR systems that use as many valves as the actuators or have narrow operating ranges like passive VR systems. The proposed design of the ORV enables orderly recruitment of multiple FAMs in the system using a single valve.

A mathematical model was developed and simulated with a rotating arm plant to characterize the dynamics of the ORV. An orderly recruitment strategy was implemented through a model-based feed forward controller. To benchmark the performance of the ORV, a conventional multi-valve system (MVS) with equivalent dynamics and controller was implemented. Trajectory tracking simulations on both the systems revealed lower tracking error for ORV compared to MVS due to the unique cross-flow effects of ORV.

However the MVS, due to its independent valve setup proved to be more adaptable for performance. For example, modifications to the recruitment thresholds of the MVS demonstrated improvement in tracking error of 20%, albeit with a sacrifice in efficiency of about 10%. In ORV tracking performance remained insensitive to any variation in recruitment threshold. This study presents the ORV design as a potential alternative to multi-valve systems with a simple setup as its advantage and marginal sacrifice in control flexibility.

© Copyright 2019 by Dheeraj Vemula

All Rights Reserved

Design and Analysis of an Orderly Recruitment Valve for Bio-inspired Fluidic Artificial
Muscles

by
Dheeraj Vemula

A thesis submitted to the Graduate Faculty of
North Carolina State University
in partial fulfillment of the
requirements for the Degree of
Master of Science

Mechanical Engineering

Raleigh, North Carolina
2019

APPROVED BY:

Dr. Gregory Buckner

Dr. Katherine Saul

Dr. Matthew Bryant
Chair of Advisory Committee

BIOGRAPHY

Dheeraj Vemula was born in Machalipatnam and raised in Vijayawada, India. He received a dual degree in Engineering Design and Automotive Engineering from Indian Institute of Technology, Madras in 2014. Upon graduation, he worked as a senior CAE engineer at General Motors till 2016. He began his graduate studies in Mechanical Engineering at North Carolina State University and will receive his Masters degree in Fall 2019.

ACKNOWLEDGEMENTS

I would first like to acknowledge Dr. Gregory Buckner, Dr. Katherine Saul and Dr. Matthew Bryant for their involvement in my graduate committee. Additionally, I want to thank Dr. Matthew Bryant for providing me the opportunity to work on this project and his continual guidance throughout the research. I would like to express my gratitude to the members of ISSRL at NC State University and my friends for their insightful comments and encouragement for the past 2 years. Finally, I must express profound gratitude to my parents and sister for providing me with unfailing support and continuous encouragement throughout my years of study.

TABLE OF CONTENTS

List of Tables	v
List of Figures	vi
Chapter 1 INTRODUCTION	1
1.1 Fluidic Artificial Muscle background	1
1.2 Variable Recruitment in FAMs	3
1.2.1 Active Variable Recruitment	3
1.2.2 Passive Variable Recruitment	4
1.2.3 Research Objectives	5
Chapter 2 System Modeling	6
2.1 Valve Modeling	7
2.1.1 Design of the Orderly Recruitment Valve	7
2.1.2 Flow Dynamics	9
2.1.3 Spool Dynamics	10
2.2 Fluidic Artificial Muscle Modeling	11
2.2.1 FAM Force Characterisation	11
2.2.2 FAM Pressure Dynamics	12
2.3 Rotating Arm Plant Modeling	13
2.4 Hydraulic Power Unit Modeling	14
Chapter 3 Orderly Recruitment and Controller Implementation	17
3.1 Orderly Recruitment	17
3.2 Controller implementation	18
3.2.1 Feed forward controller with orderly recruitment	19
Chapter 4 Results and Discussion	22
4.1 Recruitment Phase	23
4.2 Comparison of ORV and Multi-valve system	26
4.3 Tracking Enhancement with Modified Switching Logic	28
4.4 System with Different Valve Configurations	30
Chapter 5 CONCLUSIONS	34
5.1 Future Work	35
References	37
APPENDIX	39
Appendix A Acronyms and Variables	40

LIST OF TABLES

Table 2.1	Parameters used for different subsystems	16
Table A.1	A summary of acronyms used in alphabetical order.	40
Table A.2	A summary of common variables in alphabetical order.	41

LIST OF FIGURES

Figure 2.1	Schematic with different subsystems in the model	7
Figure 2.2	Schematic showing different phases of the orderly recruitment valve	8
Figure 2.3	Orderly recruitment valve geometry	9
Figure 3.1	Block diagram showing the control structure of the feed forward PI controller along with different signal flows in the system	21
Figure 4.1	Simulation results for a trajectory of 0.15 Hz frequency with $\Delta\theta = 45^\circ$ (a) shows a comparison of the system arm angle rotation with the reference trajectory. (b) shows the normalized position of the trailing end of the spool during the simulation	23
Figure 4.2	Simulation results for a trajectory of 0.15 Hz frequency with $\Delta\theta = 45^\circ$ (a) shows the pressure dynamics in FAM 1 and FAM 2 during the simulation, highlighting their important characteristics during the recruitment phase. (b) shows the FAM forces and the drop in FAM 1 force during the recruitment phase	24
Figure 4.3	Different states of the FAM 1 and FAM 2 during the simulation highlighting the slack state FAM 2 during the recruitment phase	25
Figure 4.4	Schematic of the independent valve configuration of the multi-valve system	26
Figure 4.5	A simplified block diagram of a control system used to implement a model-based feed forward PI controller in the multi-valve system	27
Figure 4.6	Trajectory tracking performance ORV and MVS over a range of frequencies	28
Figure 4.7	Trajectory tracking performance ORV and MVS over a range of frequencies	29
Figure 4.8	Trajectory tracking performance of MVS and ORV over a range of frequencies and threshold factors	31
Figure 4.9	Efficiency of MVS and ORV systems over a range of frequencies and threshold factors	32

CHAPTER

1

INTRODUCTION

1.1 Fluidic Artificial Muscle background

McKibben artificial muscles or fluidic artificial muscles (FAMs) were first created by their namesake Joseph McKibben as an orthopedic aid for his polio stricken daughter (19). Inspired from mammalian muscles, FAMs share many similarities with their mammalian counterparts. Just as mammalian muscles are activated by an applied activation energy, FAMs are activated by an applied pressure. Similar to mammalian muscles, FAMs are single-acting contractile actuators with an inverse force-strain behavior (16). Since FAMs are single-acting, they need an antagonist pair to act as a double-acting actuator. A typical

FAM construction is inexpensive and primarily consists of two concentric elements, the inner component is an elastic bladder embedded within a pantograph structured braided mesh. When pressurized, this bladder expands into the mesh pushing it radially outwards. The outer mesh, due to its pantograph structure, expands radially while contracting axially thus producing a contractile force. The force-strain behavior of a FAM is governed by the applied pressure and the FAMs construction geometry such as the initial radius, length and braid angle. Therefore, a wide range of force-strain profiles can be obtained by altering the applied pressure or the construction of the FAM.

FAMs are popular and widely studied due to their inherent compliance, low cost, large displacements, high force-to-weight ratio and similarity to mammalian muscles in actuation ((15), (24)). (18) compared an antagonist pair of FAMs to an equivalent double-acting cylinder and found that FAMs were able to achieve a force-to-weight ratio that is six times greater at $1/10^{th}$ the price of a cylinder. These advantages present artificial muscles as an attractive option for actuation in humanoid ((20)), prosthetic and rehabilitation robots ((1), (4), (9), (17)). Until recently researchers have been studying pneumatic FAMs. However since these systems use compressed air as operating fluid, pneumatic FAMs present certain limitations on performance characteristics such as response time when compared to traditional piston cylinder actuators (22). In addition, due to characteristics inherent to pneumatic systems such as high compressibility and leakage, these systems tend to have lower efficiency.

(13) compared hydraulic and pneumatic actuation of FAMs and found that hydraulic FAMs present both performance and efficiency advantages. Hydraulic FAMs have found to be 180% more energy efficient in producing the same amount of mechanical energy while considering the energy required to compress the working fluid. This trait in hydraulic FAMs has been attributed to lower compressibility of hydraulic fluid when compared to pneumatic fluid such as air. Hydraulic FAMs also typically have higher stiffness that varies

linearly with pressure when compared to the non-linear drive characteristics of pneumatic artificial muscles. This enables easier and better position control for hydraulic FAMs.

1.2 Variable Recruitment in FAMs

In mammalian muscles, individual muscle fibers are bundled together to form larger muscle units (3). The individual muscles within the larger bundles are recruited based on Henneman's size principle, which states that muscle fibers are recruited in an orderly fashion from smaller units to larger units as load requirement increases (7). Employing a similar principle in FAM bundles, researchers have shown a two-fold improvement in efficiency with a variable recruitment muscle bundle when compared to a single equivalent motor unit (SEMU) (2). This strategy uses the least number of individual muscles or motor units within the bundle that are required based on the applied load and enables most of the motor units to be at ideal operating pressure while minimizing the fluid volume consumption and throttling losses. This variable recruitment principle has been implemented primarily through two different methodologies, passive variable recruitment (PVR) and active variable recruitment (AVR), both of which are discussed in the following sections.

1.2.1 Active Variable Recruitment

In AVR, the individual motor units are controlled independently through the control valves dedicated to them. This "multi-valve" configuration is inherently flexible and can be tailored to function over a wide range of operating conditions. (11) implemented an online active variable recruitment strategy with a multi-valve system (MVS) to control FAM bundle with 3 pairs of muscles. The researchers incorporated three recruitment levels in the muscle bundle. Progression from lower recruitment level to higher recruitment level would happen

when the current muscle reaches saturation i.e. reaches the source pressure. The recruitment pressure can be tailored to the required load and thus can be operated at maximum efficiency for a wide range of loads. However with a multi-valve configuration, the system requires as many valves as the number of motor units within the system. This increases complexity and weight of the entire system which can be detrimental in applications such as mobile robotics or wearable exoskeletons where artificial muscle systems are being widely used.

1.2.2 Passive Variable Recruitment

A system with PVR uses difference in the mechanical design of the individual motor units within a muscle bundle to achieve variable recruitment (5). Akin to threshold energy that is required for activation of the muscle fiber in mammalian muscles, FAMs require a minimum pressure termed as threshold pressure to start generating contraction. This threshold pressure for a FAM is derived based on the geometry and material properties of the FAM. A FAM system with PVR consists of a control valve that controls the pressure to the bundle and multiple motor units with distinct threshold pressures. When applied with certain pressure all the muscles whose threshold pressure is less than the applied pressure are activated. Chapman and Bryant (5) showed that a PVR bundle is more efficient compared to a single equivalent motor unit in low load conditions. This strategy has been shown to be advantageous since it uses a single control valve for the entire bundle. However, a very high threshold pressure in the mechanical design means that greater energy elastic energy is stored in the the actuator reducing the actual work output of the system. This implies restrictions on threshold pressures in terms of efficiency which can lead to narrow lower threshold pressures and thus narrower operating ranges.

1.2.3 Research Objectives

The research presented in this paper focuses on the design and analysis of an orderly recruitment valve (ORV) that offers the control flexibility similar to AVR with the simplicity of a single valve in PVR. In chapter 2, complete analytical model of a one degree of freedom robotic arm with hydraulic FAM actuators using the ORV is presented. In chapter 3, A model-based feed-forward control system is developed to control the valve system to track a prescribed trajectory. Chapter 4 provides results and discussions of the trajectory tracking simulations for the ORV and a comparative study of the ORV with an equivalent multi-valve system. Performance characteristics such as efficiency and integrated absolute error are evaluated across a range of trajectories. Lastly, conclusions summarizing the modeling and trajectory tracking simulations were presented in Chapter 5 along with the scope for future work.

CHAPTER

2

SYSTEM MODELING

A single degree of freedom rotating arm consisting of the following subsystems, as illustrated in Figure 2.1, was developed and simulated.

1. ORV
2. Actuation system with two FAM actuators
3. A rotating arm assembly with a pulley, arm and an end mass
4. Hydraulic power unit with a motor-pump assembly and an accumulator

Analytical models for each of these subsystems are developed to simulate the overall system dynamics. These models were later used to simulate and compare the performance

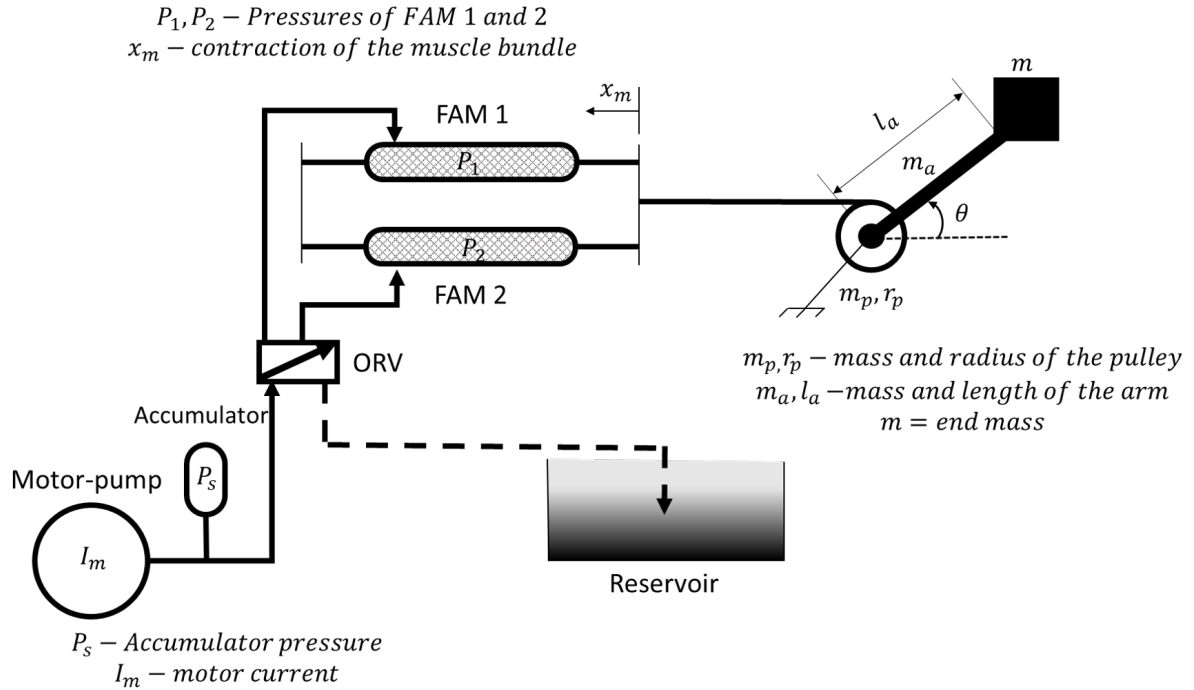


Figure 2.1: Schematic with different subsystems in the model

of the ORV with a conventional multi-valve setup that is required for active variable recruitment.

2.1 Valve Modeling

2.1.1 Design of the Orderly Recruitment Valve

The design goal of the ORV is to enable actuation of multiple FAMs sequentially. For the purpose of demonstration, a simple design (illustrated in Figure 2.2) for the ORV that can work with two FAMs is proposed and simulated. The ORV assembly primarily consists of two components, a valve body and a spool. The valve body consists of a supply port, a reservoir port and 2 ports for the FAM units. The FAM ports are normally venting to the reservoir and as the spool travels from left of the valve body to the right, it opens the FAM

ports to the supply port while sequentially pressurizing them.

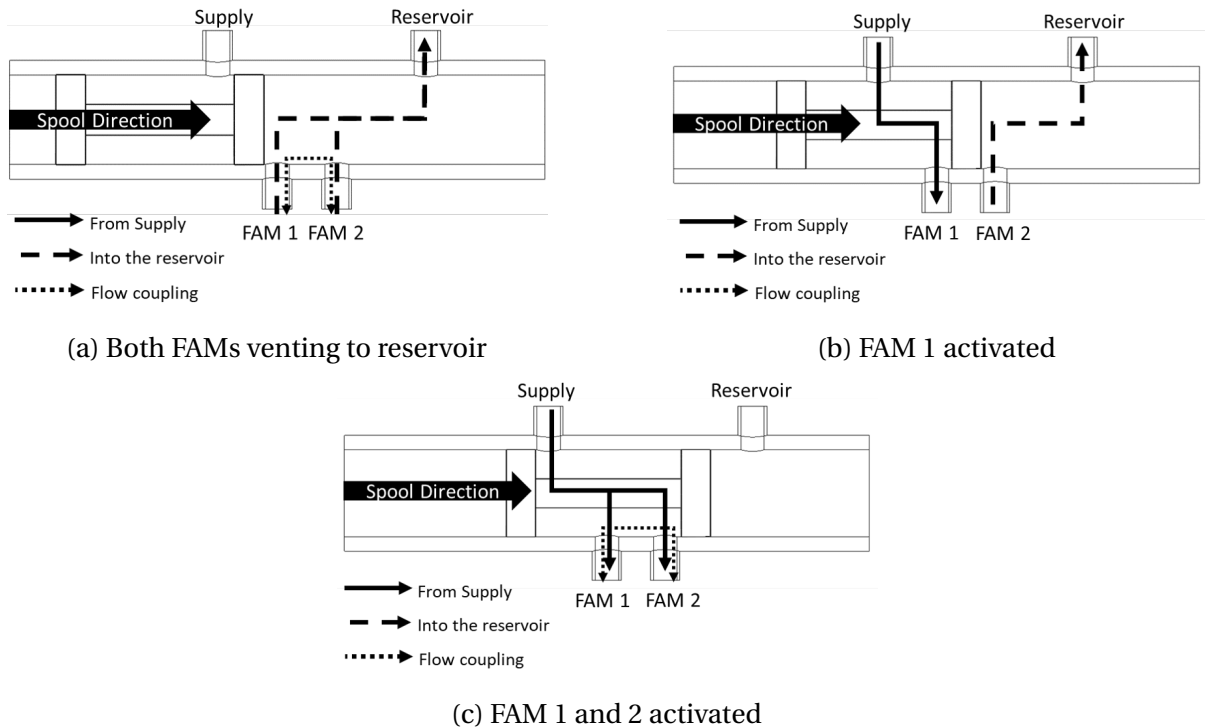


Figure 2.2: Schematic showing different phases of the orderly recruitment valve

The simplicity of the proposed design facilitates an easy extension for any number of FAMs depending on the system requirement. To extend the ORV there can be an increased number of ports between the supply port and reservoir port, which can be connected to multiple FAMs. This layout of the ORV introduces a unique geometric element in its dead band, x_{db} . The dead band is defined as the clearance between two consecutive FAM input ports. For the sake of simplicity, an ORV that can operate two FAM motor units is presented throughout this paper.

The ORV geometry as shown in Figure 2.3 is assumed to be critically lapped which means that the spool width, x_{sw} is equal to the port opening diameters, $x_{v,1}$ and $x_{v,2}$ (10).

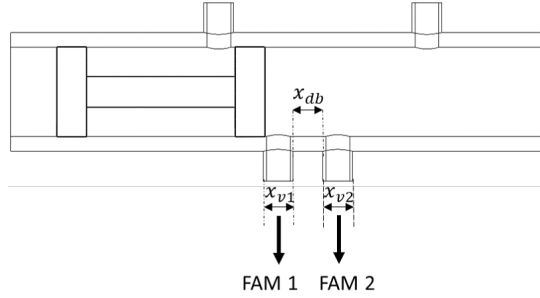


Figure 2.3: Orderly recruitment valve geometry

The dead band, x_{db} is sized to avoid any overlap between ports during operation thus making it equal to the spool width. By transitive relation this makes the dead band equal to port diameters as shown in Equation 2.1.

$$x_{v,1} = x_{v,2} = x_{sw} = x_{db} \quad (2.1)$$

In order to effectively characterize the performance of the ORV, an analytical model is developed that emulates the pressure flow dynamics and the spool dynamics. The valve is sized and modeled based on a commercial servo valve, MOOG G761 (MOOG) and all the required parameters for the valve model are obtained from the manufacturer's catalogue of the MOOG valve.

2.1.2 Flow Dynamics

Due to its design, the ORV exposes multiple FAM ports to each other during actuation when the spool is at extreme positions as shown in Figures 2.2a and 2.2c. In addition to traditional flow between the supply and input ports or input and reservoir ports, the ORV introduces flow coupling between multiple FAM input ports termed as 'cross-flow'. This cross-flow across FAMs occurs whenever there is a pressure differential, which happens during the transient phase of the variable recruitment. This is evident in the flow equations for the

valve which is modeled based on orifice flow. As described in Equation 2.4, the cross-flow term, Q_{cf} is a function of the individual FAM pressures, P_1 and P_2 , accumulator pressure, P_s , flow coefficient, c_v and the port openings, $x_{v,1}$ and $x_{v,2}$.

$$Q_1 = c_v x_{v,1} \text{sgn}(P_s - P_1) \sqrt{|P_s - P_1|} - Q_{cf} \quad (2.2)$$

$$Q_2 = c_v x_{v,2} \text{sgn}(P_s - P_2) \sqrt{|P_s - P_2|} + Q_{cf} \quad (2.3)$$

$$Q_{cf} = c_v \max(x_{v,1}, x_{v,2}) \sqrt{|P_1 - P_2|} \text{sgn}(P_1 - P_2) \quad (2.4)$$

The flow coefficient, c_v is calculated as shown in Equation 2.5 based on the nominal flow data of the valve.

$$c_v = \frac{Q_N}{\sqrt{\Delta p_N/2}} \frac{1}{x_{v,max}} \quad (2.5)$$

where Q_N is the nominal flow, Δp_N is the nominal pressure drop, and $x_{v,max}$ is the maximum stroke of the valve.

2.1.3 Spool Dynamics

The spool travel in the ORV determines different recruitment levels for the FAM, therefore the spool dynamics are vital in understanding the dynamics of the ORV. A second order system is used to model the spool dynamics for the ORV (8). The spool position, x_v is dependent on the valve parameters such as natural frequency, ω_v , gain, K_v , damping coefficient, D_v , hysteresis, f_{hs} and the input signal, u_v .

$$\frac{1}{\omega_v^2} \ddot{x}_v + \frac{2D_v}{\omega_v} \dot{x}_v + x_v + f_{hs} \text{sign}(\dot{x}_v) = K_v u_v \quad (2.6)$$

A full stroke motion in a traditional valve ranges from the opening to closing of one port, however the ORV has two ports as it controls two FAM units. Therefore the full stroke of the ORV should range from the opening of the first port to the closing of the second port which also includes the dead band region in between the two ports. Since the dimensions of the ports are assumed to be identical and are equal to that of the dead band, the total stroke for the ORV is thrice that of a traditional valve.

2.2 Fluidic Artificial Muscle Modeling

2.2.1 FAM Force Characterisation

For this research, an ideal FAM model is considered which approximates the shape of the muscle to a perfect cylinder and also assumes the intrinsic mechanical properties of the braided outer mesh and the inner elastic tube to be negligible. Researchers (21) have developed a geometric model for ideal muscles that establishes a relation between the FAM contraction, x_m , the FAM volume, V_m and the initial FAM geometry such as the length, l_0 , radius, r_0 and braid angle, α_0 as shown in Equations 2.7 and 2.8.

$$V_m = \pi r_0^2 l_0 \left[b \left(1 - \frac{x_m}{l_0} \right) - a \left(1 - \frac{x_m}{l_0} \right)^3 \right] \quad (2.7)$$

$$a = \frac{3}{\tan \alpha_0^2}, b = \frac{1}{\sin \alpha_0^2} \quad (2.8)$$

An ideal FAM model is developed based on the virtual work principle that relates the fluid energy to the mechanical work done as shown in Equation 2.9

$$P \delta V_m = F \delta x_m \quad (2.9)$$

where F_m is the axial force output of the FAM, δx_m is the FAM contraction along the line of action of the force, P is the FAM pressure and δV_m is change in the FAM volume. Differentiating the muscle volume, V_m with respect to the FAM contraction, x_m and rearranging Equation 2.9 for force yields the relation between muscle force, pressure, geometry and contraction as shown in Equation 2.10.

$$F_m = \pi r_0^2 P \left[a \left(1 - \frac{x_m}{l_0} \right)^2 - b \right] \quad (2.10)$$

2.2.2 FAM Pressure Dynamics

The transient phase of variable recruitment is important to precisely evaluate the dynamics of the system. The pressure dynamics of the FAM influence its force and consequently the overall plant dynamics. The pressure growth in the FAM is due to the compression of fluid volume in the muscle. Assuming isothermal compression of the fluid, as the volume rate of fluid into the muscle is greater than the volume rate of change of the muscle, pressure within the muscle grows as shown in Equation 2.11

$$\frac{dP}{dt} = \frac{1}{\beta} \frac{Q - \dot{V}_m}{V_m} \quad (2.11)$$

$$\dot{V}_m = \pi r_0^2 \left[a \left(1 - \frac{x_m}{l_0} \right)^2 - b \right] \dot{x}_m \quad (2.12)$$

where β is the compressibility of fluid and \dot{V}_m is the rate of change of the FAM volume. \dot{V}_m is a function of the FAM contraction velocity, \dot{x}_m and is obtained by differentiating FAM volume (Equation 2.7) w.r.t time as shown in Equation 2.12. Since the range of operating

pressures in the FAM is small enough (0–750 kPa), β is assumed to be constant throughout the pressure growth cycle of the FAM.

2.3 Rotating Arm Plant Modeling

A rotating arm plant is chosen to simulate varying loads on the muscle bundle to trigger recruitment of different muscles. As illustrated in Figure 2.1, the plant consists of a rotating robotic arm-pulley assembly with a mass at the tip. The pulley of mass, m_p and radius, r_p is connected to a FAM bundle consisting of two FAMs. The contractile force, F_{bundle} of the FAM bundle translates into a torque on the pulley which is counteracted by an external torque, τ_{load} due to the mass of the robotic arm, m_a and the tip mass, m . The equations of motion of the system relating the FAM forces and the angular displacement of the arm, θ are given in Equations 2.13 and 2.14 where I is the moment of inertia of the system and c is the damping within the system.

$$\tau_{net} = F_{bundle} r_p - \tau_{load} = I \ddot{\theta} + c \dot{\theta} \quad (2.13)$$

$$\tau_{load} = m g l_a \cos \theta + m_a g \frac{l_a}{2} \cos \theta \quad (2.14)$$

The bundle contraction, $x_{m,bundle}$ and arm angle are related as shown in Equation 2.15.

$$x_{m,bundle} = l_0 - r_p \theta \quad (2.15)$$

2.4 Hydraulic Power Unit Modeling

The hydraulic subsystem comprises of a pressure source and an incompressible hydraulic fluid. The pressure source consists of a motor-pump assembly connected to an accumulator that governs the inlet pressure for the valve system. Modeling the dynamics of the motor pump assembly and the accumulator is essential to simulate the dynamics of supply pressure to the FAMs. Due to the volume consumed by the FAMs during contraction, there is a drop in the pressure of the accumulator, P_s which is modeled using ideal gas law while assuming that the temperature is constant as shown in Equation 2.16.

$$P_s = \frac{P_{si} V_{si}}{V_{si} + (V_{m,1} + V_{m,2}) - V_p} P_{si} V_{si} = P_s (V_{si} + (V_{m,1} + V_{m,2}) - V_p) \quad (2.16)$$

P_{si} and V_{si} are the initial pressure and volume of the gas charged accumulator, $V_{m,1}$ and $V_{m,2}$ are the volumes consumed by the FAMs and V_p is the volume of fluid pumped by the motor.

The motor-pump assembly which is assumed to be a positive displacement pump is under constant operation to maintain the accumulator pressure above the set pressure, hence it is important to model the motor-pump dynamics. The motor-pump dynamics are derived from first principles and Kirchhoff's voltage law as given in Equations 2.17 and 2.18.

$$\ddot{\theta}_p = \frac{K_m I_m - \tau_p}{J_p} \quad (2.17)$$

$$\dot{I}_m = \frac{V_{motor} - k_b \dot{\theta}_p - I_m R_m}{L_m} \quad (2.18)$$

The motor parameters such as current, coil inductance, coil resistance, back emf constant, torque constant and supply voltage are given by I_m , L_m , R_m , k_b , K_m and V_{motor}

respectively and the pump parameters such as the angular displacement, rotational inertia and impeller torque are given by θ_p , J_p and τ_p respectively. The parameters used in all the subsystems are listed in Table 2.1.

Table 2.1: Parameters used for different subsystems

Muscle		Accumulator	
Parameter	Value	Parameter	Value
r_0 (cm)	0.64	P_{si} (kPa)	760
l_0 (cm)	17.78	V_{si} (m^3)	0.00038
α_0 (deg)	29.67		
Motor-Pump		Rotary Arm	
Parameter	Value	Parameter	Value
L_m (H)	0.00011	m_p (kg)	1
R_m (ohms)	0.45	r_p (m)	0.05
k_b ($\frac{rad}{V.s}$)	0.017	m_a (kg)	0.5
K_m ($\frac{N.m}{A}$)	0.017	l_a (m)	1
V_m (V)	10	m (kg)	1
J ($kg m^2$)	9.45×10^{-5}	c (Ns/m)	0.029
Valve Flow		Spool Dynamics	
Parameter	Value	Parameter	Value
K_v	10	Δp_n (kPa)	350
D_v	1	Q_n (litre/s)	0.25
ω_v (Hz)	1800	$x_{v,max}$ (mm)	10.82
f_{hys} (%)	3		
Hydraulic Fluid			
Parameter	Value		
$1/\beta$ (Pa)	2.15×10^9		

CHAPTER

3

ORDERLY RECRUITMENT AND CONTROLLER IMPLEMENTATION

3.1 Orderly Recruitment

Orderly recruitment is a bio-inspired variable recruitment strategy that sequentially recruits FAM units based on the applied load. In biological musculature new motor units are recruited in a sequential manner from smaller to larger units as the load increases. Employing a similar strategy, a switching logic is used to recruit FAM units in an orderly manner based on the applied load.

The switching logic determines the recruitment state, RS based on the required pressure from the FAM bundle and the supply pressure as shown in Equation 3.1 for a FAM bundle of two units.

$$RS = \begin{cases} 1 & \text{when } P_{req} < P_s \\ 2 & \text{when } P_{req} \geq P_s \end{cases} \quad (3.1)$$

Here $RS = 1$ represents recruitment on the first FAM unit and $RS = 2$ represents recruitment of both FAM units. Pressure required is estimated based on the required force, F_{req} from the FAM and required FAM contraction, $x_{m,req}$ as shown in Equation 3.2.

$$P_{req} = \frac{F_{req}}{\pi r_0^2 \left[a \left(1 - \frac{x_{m,req}}{l_0} \right)^2 - b \right]} \quad (3.2)$$

F_{req} and $x_{m,req}$ are estimated based on the load applied (Equations 2.13, 2.14 and 2.17) and the reference position, θ_{ref} as shown in Equations 3.3 and 3.4.

$$F_{req} = \frac{I\theta_{ref}'' + c\theta_{ref}' + mgl_a \cos \theta_{ref} + m_a g(l_a/2) \cos \theta_{ref}}{r_p} \quad (3.3)$$

$$x_{m,req} = l_0 - \theta_{ref} r_p \quad (3.4)$$

3.2 Controller implementation

There is an abundance of literature on controller development for pneumatic artificial muscles (6), with more recent developments in control systems for hydraulic artificial muscles (23).

(12) developed a model-based feed forward PI controller for hydraulic artificial muscle system with variable recruitment that can improve performance tracking due to its ability to take predictive action. However, this implementation uses linearization to identify the flow gain of the controller for a commanded input signal to the valve. Due to the transient phase in the orderly recruitment used in the current research, the linearization approximation does not consider the pressure dynamics. Inspired from the linearized feed forward controller and the gap in its approximations, an updated controller is developed to suit the orderly recruitment strategy.

3.2.1 Feed forward controller with orderly recruitment

The objective of the updated controller is to address the linearization approximations through an inverse dynamics model that is used to estimate the relation between spool position and reference trajectory. This controller development was initially established for a FAM bundle consisting of a single FAM unit and later extended to FAM bundles with multiple motor units for variable recruitment.

Feed forward input estimation

The feed forward model needs two stages of parameter estimation to accurately provide a feed forward input. The first stage is pressure estimation from Equation 3.2 and second stage is the required valve input estimation. After estimating the required pressure as shown in Equation 3.2, the next step is to estimate the required spool position, $x_{v,req}$ based on the estimated pressure and required flow rate, $Q_{m,req}$ as shown in Equation 3.5

$$x_{v,req} = \frac{Q_{m,req}}{c_v \sqrt{|P_{s,req} - P_{req}|} \text{sgn}(P_{s,req} - P_{req})} \quad (3.5)$$

where $Q_{m,req}$ is the required flow rate from the valve and $P_{s,req}$ is the required supply

pressure. $Q_{m,req}$ is estimated based on the required FAM contraction as shown in Equation 3.6 and $P_{s,req}$ is a function of hydraulic subsystem's initial states and the reference trajectory.

$$Q_{m,req} = \pi r_0^2 \left[a \left(1 - \frac{x_{m,req}}{l_0} \right)^2 - b \right] \dot{x}_{m,req} \quad (3.6)$$

After estimation of the required spool position, the corresponding valve feed forward input, u_{ff} is calculated based on inverting the spool dynamics from Equation 2.6 as shown in Equation 3.7.

$$u_{ff} = \frac{\left[\frac{1}{\omega_v^2} x_{v,req}'' + \frac{2D_v}{\omega_v} \dot{x}_{v,req} + x_{v,req} + f_{hs} \text{sign}(\dot{x}_{v,req}) \right]}{K_v} \quad (3.7)$$

The feed forward estimation for a single FAM shown above is extended for a FAM bundle based on the recruitment state, RS . A PI feedback loop is added to this feed forward controller whose overall control law is shown in Equation 3.8

$$u_v = u_{ff} + u_{pi} \quad (3.8)$$

where the PI control input, u_{pi} is a function of the PI gains and the trajectory error, e as shown in Equations 3.9 and 3.10 respectively.

$$u_{pi} = K_p e + K_i \int e \quad (3.9)$$

$$e = \theta_{ref} - \theta \quad (3.10)$$

As shown in Figure 3.1, the overall control architecture of the system consists of six primary blocks. The control structure developed in this chapter is used to control the system model developed in the previous chapter to track a prescribed trajectory. These trajectory

tracking simulations were used to characterize the behavior of the ORV.

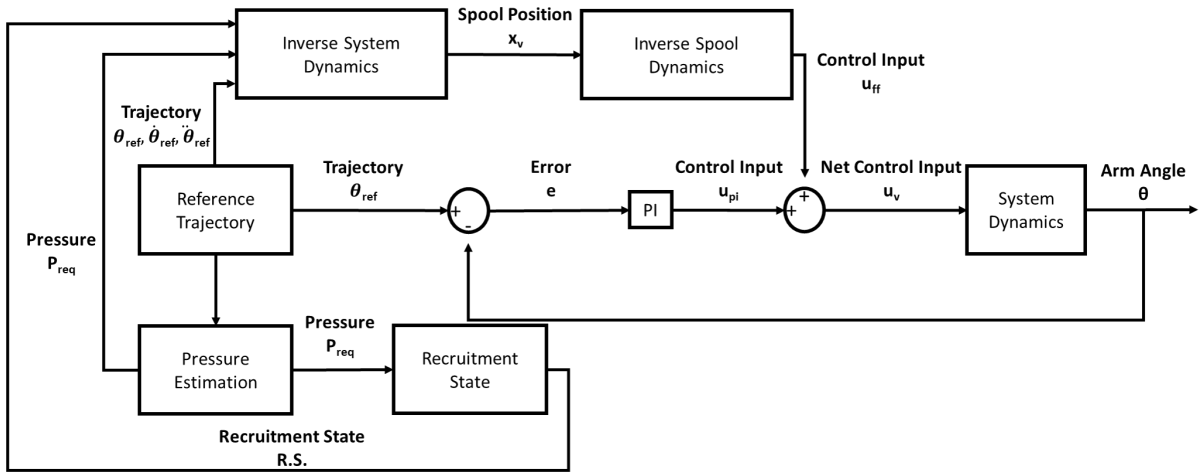


Figure 3.1: Block diagram showing the control structure of the feed forward PI controller along with different signal flows in the system

CHAPTER

4

RESULTS AND DISCUSSION

To illustrate the dynamics of the system and demonstrate characteristics of the ORV, a series of trajectory tracking simulations for the rotating arm angle are developed. Half-sine trajectories with varying frequencies are used to simulate a parametric case study. The feed forward PI controller developed in Section 3.2.1 is used to track the reference trajectories. Since the objective of this study was to characterize the ORV, the controller was assumed to be ideal with zero modeling errors. The gains for the PI controller ($K_p = 53.1 V/rad$, $K_i = 27.2 V/rad$) were tuned based on Ziegler-Nichols method with further refinement through hand tuning.

4.1 Recruitment Phase

A half-sine trajectory with a frequency of 0.15 Hz (which translates into a time span, $\Delta t = 3.33\text{ s}$) with reference arm angle, $\Delta\theta$ of 45° with arm angle travel from -45° to 0° is simulated. FAM 1 was initialized with a pressure just enough to start the simulation from an equilibrium. A tip mass ($m = 1\text{ kg}$) is chosen so that the first FAM reaches saturation at an arm angle of -9.0° degrees, at which the second muscle recruitment begins. Integrated absolute error (IAE), e_{IAE} as defined in Equation 4.1, was used to quantify the overall tracking accuracy of the system. The ORV system tracked the reference trajectory shown in Figure 4.1a with an $e_{IAE} = 2.5899\text{ rads}$.

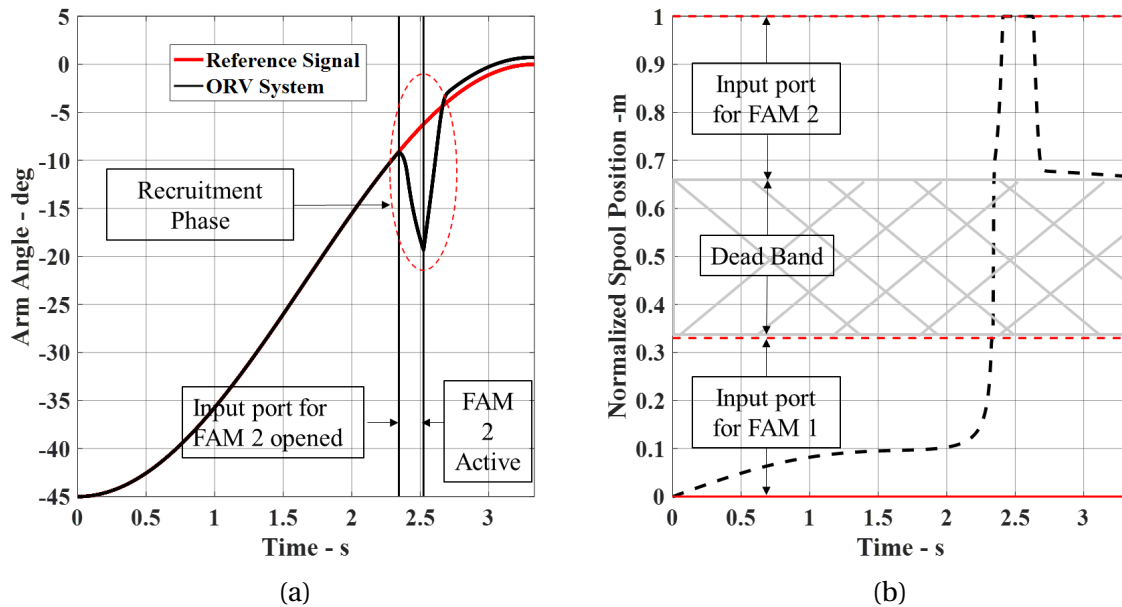


Figure 4.1: Simulation results for a trajectory of 0.15 Hz frequency with $\Delta\theta = 45^\circ$ (a) shows a comparison of the system arm angle rotation with the reference trajectory. (b) shows the normalized position of the trailing end of the spool during the simulation

$$e_{IAE} = \int |\theta_{ref} - \theta| \quad (4.1)$$

Results from the simulation shown in Figure 4.1a highlight accurate tracking until recruitment of the second FAM. This accuracy can be attributed to the ideal model assumption in the feed forward controller. However, during the recruitment of the second muscle we can see that the arm experiences a significant "dip" of 10^0 . There are two important physical

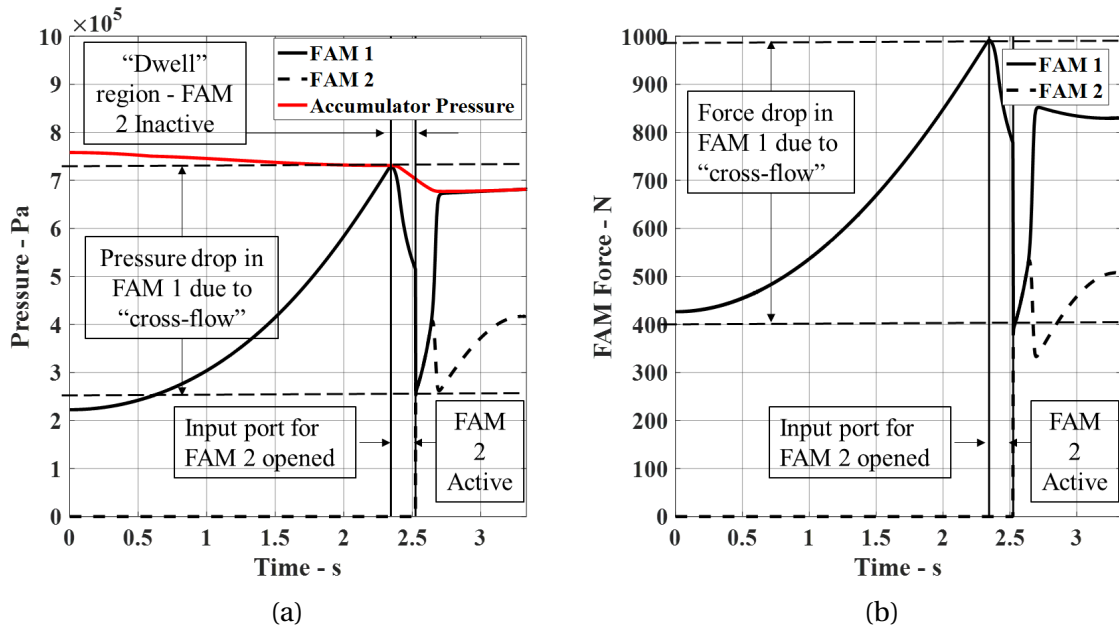


Figure 4.2: Simulation results for a trajectory of 0.15 Hz frequency with $\Delta\theta = 45^\circ$ (a) shows the pressure dynamics in FAM 1 and FAM 2 during the simulation, highlighting their important characteristics during the recruitment phase. (b) shows the FAM forces and the drop in FAM 1 force during the recruitment phase

phenomena that occur during the phase corresponding to this dip. The first of these phenomena is the "dwell" state of FAM 2 where it does not get pressurized even though it is recruited as shown in Figure 4.2a. Figure 4.3 shows that at the beginning of dwell state, FAM 2 is "slack" since it has zero contraction and FAM 1 is at a contraction level corresponding

to the arm angle, θ . This leads to a free-strain contraction, x_{free} (Equation 4.2) of FAM 2 until it "de-slacks" to the contraction level of FAM 1 during which it does not exert any force as seen in Figure 4.3.

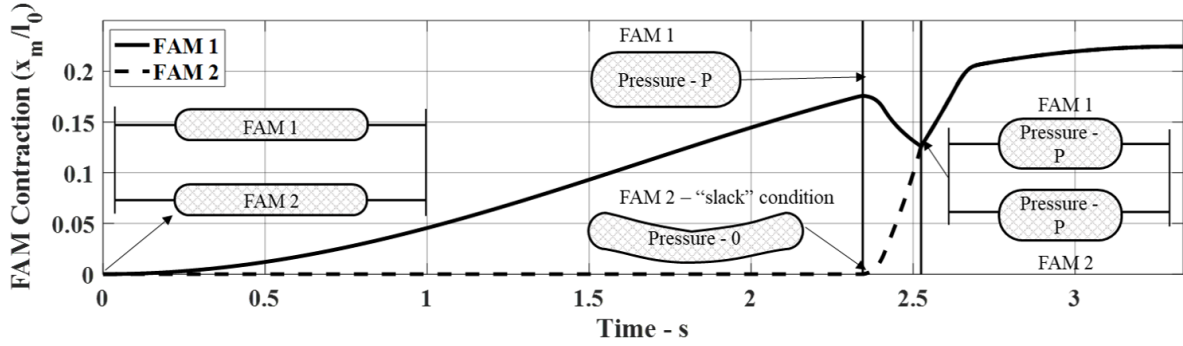


Figure 4.3: Different states of the FAM 1 and FAM 2 during the simulation highlighting the slack state FAM 2 during the recruitment phase

$$\dot{x}_{free} = \frac{c_v x_{v,2} \sqrt{P_s} + Q_{f,12}}{\pi r_0^2 \left[a \left(1 - \frac{x_{free}}{l_0} \right)^2 - b \right]} \quad (4.2)$$

Here $x_{v,2}$ is the port opening for input port of FAM 2, P_s is the supply pressure and Q_{cf} is the cross flow between the FAM units as given in Equation 4.3

$$Q_{f,12} = c_v x_{v,2} \sqrt{P_1} \quad (4.3)$$

where P_1 is the pressure in FAM 1.

The other important phenomenon that occurs during the recruitment phase is the drop in the pressure of FAM 1 which corresponds to a drop in muscle force as well which is shown in Figure 4.2b. This is due to the cross-flow, Q_{cf} between the FAM ports during FAM 2 recruitment. It can be seen in Figure 4.1b that the spool position is at the closing point of FAM 2's input port which results in complete opening of FAM 1's input port. Since this

occurs during the dwell phase of FAM 2, it creates a pressure differential across the FAM units which results in fluid flow from FAM 1 to FAM 2 resulting in a pressure drop in FAM 1.

4.2 Comparison of ORV and Multi-valve system

Existing research for variable recruitment in hydraulic artificial muscles uses multiple valves to control a FAM bundle. The ability of a Multi-Valve System (MVS) to control the FAM units independently makes this system ideal in terms of performance. The cross-flow effect seen in ORV is absent in MVS as the FAM units are decoupled from each other.

An MVS with two independent and identical valves whose spool dynamics and sizing are equivalent to the ORV described in Section 2.1.1 is shown in Figure 4.4. To compare both the valve systems, they are coupled with identical rotating arm FAM systems. In addition to identical plant models, equivalent controllers are also required to isolate the effects of the valve systems. Since an MVS has two valves, there are two controllers in the control system. The feed forward controller developed in Section 3.2.1 for single FAM unit remains relevant for the MVS since the individual system dynamics are identical in both the ORV and MVS. Hence, two identical feed forward controllers are implemented for both the valves in the MVS as shown in Figure 4.5.

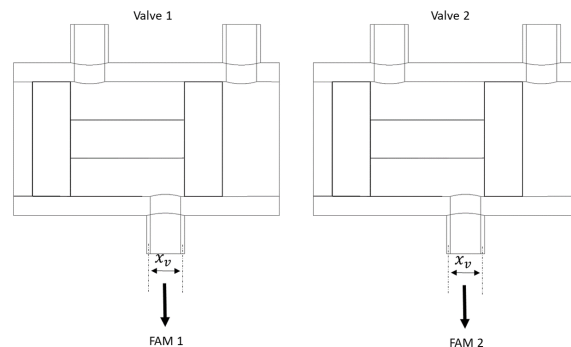


Figure 4.4: Schematic of the independent valve configuration of the multi-valve system

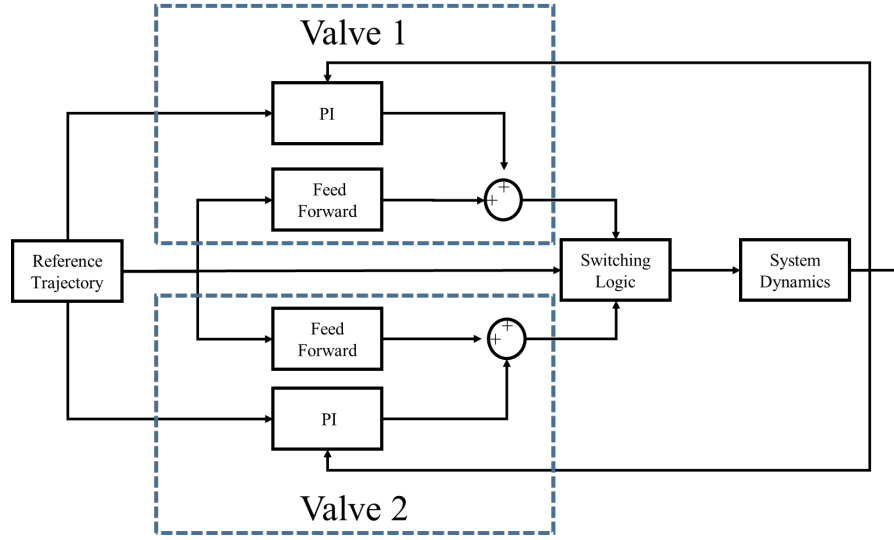


Figure 4.5: A simplified block diagram of a control system used to implement a model-based feed forward PI controller in the multi-valve system

The orderly recruitment strategy dictates that one active valve controls the active FAM unit while the other valve is passive. Therefore the control laws for the valves are designed based on the recruitment state such that the active valve gets the feed forward PI control input, u_v while the passive valve continues at its previous control state u^{prev} as shown in Equations 4.4 and 4.5.

$$u_{mv,1} = \begin{cases} u_v & \text{when } RS = 1 \\ u_{mv,1}^{prev} & \text{when } RS = 2 \end{cases} \quad (4.4)$$

$$u_{mv,2} = \begin{cases} u_{mv,2}^{prev} & \text{when } RS = 1 \\ u_v & \text{when } RS = 2 \end{cases} \quad (4.5)$$

Figure 4.6a shows a trajectory tracking comparison between ORV and MVS which reveals that the ORV performs better compared to the MVS. The primary driver for these results is the dwell region in the recruitment phase. The dwell region of MVS is longer compared to that of the ORV. This is because of the cross-flow in the ORV which leads to a faster

pressurization of FAM 2. The free strain contraction in the MVS is only due to the supply pressure whereas in the ORV both the supply and FAM 1 contribute. Also, FAM 2 has lesser slack to overcome before pressurizing in the ORV system as FAM 1 itself slacks during the recruitment phase.

Further a series of trajectories with an arm angle rotation of 45° and varying in frequencies ranging from 0.05 Hz to 0.3 Hz are simulated for both the valve systems. These simulations show that the ORV consistently performs better compared to the MVS.

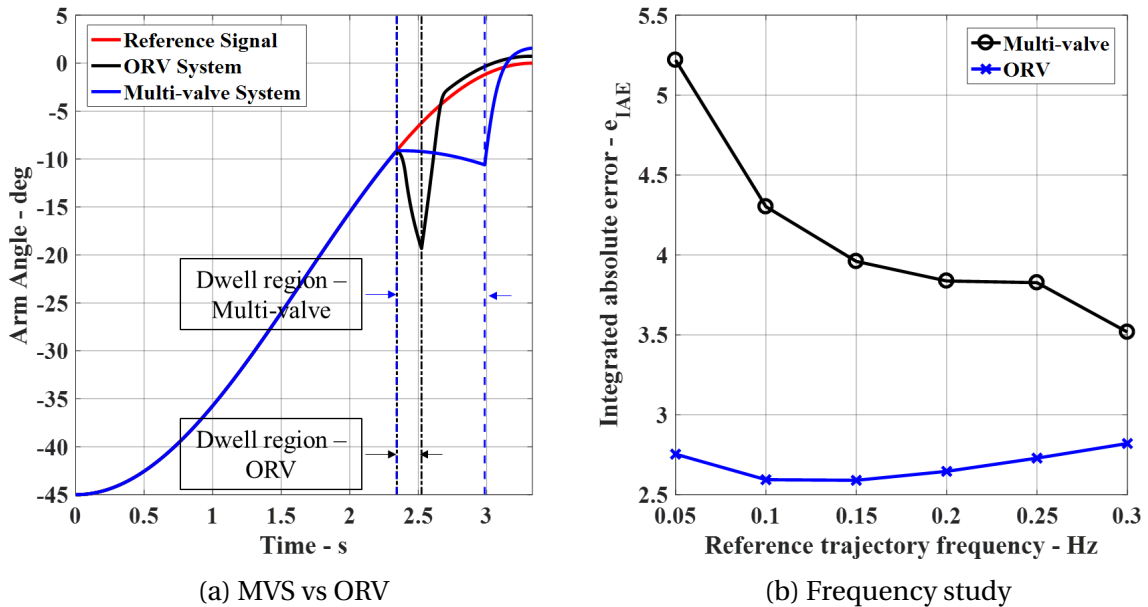


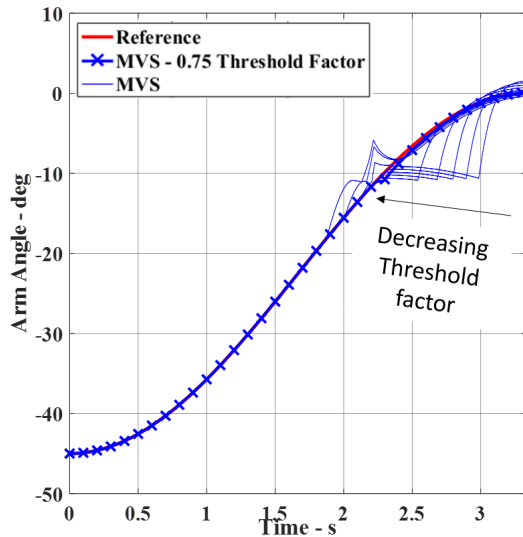
Figure 4.6: Trajectory tracking performance ORV and MVS over a range of frequencies

4.3 Tracking Enhancement with Modified Switching Logic

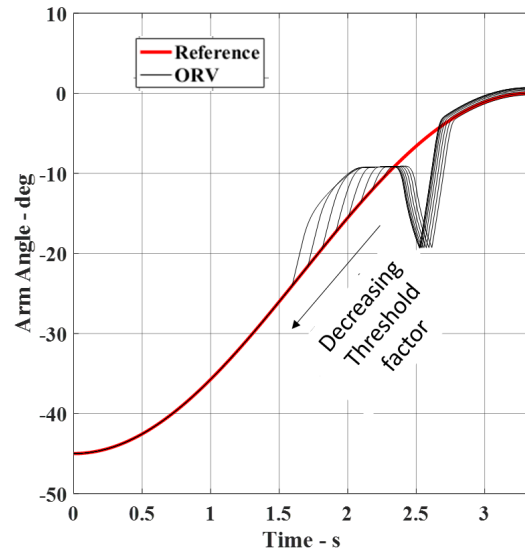
The current switching logic determines that the recruitment of FAM 2 happens when FAM 1 reaches its maximum capacity i.e. when the required pressure is equal to the supply

pressure. In the modified switching logic a threshold factor, k_{th} ranging from 0 to 1 is introduced to advance the recruitment point. With the threshold factor the recruitment for FAM 2 happens when the required pressure reaches $k_{th}P_s$ as shown in Equation 4.6. The lower the k_{th} , the earlier the recruitment for FAM 2 happens thus pressurizing it ahead of when it is required. A parametric study is carried out over a range of threshold factors and frequencies for the trajectories to identify the performance gains in trajectory tracking.

$$RS_{modified} = \begin{cases} 1 & \text{when } P_{req} < P_{th} \\ 2 & \text{when } P_{req} \geq P_{th} \end{cases} \quad (4.6)$$



(a) Multi-valve system



(b) Orderly recruitment valve

Figure 4.7: Trajectory tracking performance ORV and MVS over a range of frequencies

The threshold factor for a trajectory with a frequency of 0.15 Hz reveals that the performance gains of MVS over ORV due to its control flexibility, while the ORV's performance degrades as the threshold factor decreases. Due to the design of the ORV, the input port

for FAM 1 opens completely when recruiting FAM 2 thus rapidly increasing the pressure in FAM 1. Although the threshold factor enables earlier recruitment of FAM 2 by shifting the recruitment point, the gains due to this advancement seem to be negated by the overshoot caused by the accelerated pressure growth in FAM 1 (Figure 4.7b). There is a flexibility in control law for MVS since the passive valve can be maintained at its previous control input. This allows for the valve of FAM 1 to maintain its previous state when FAM 2 is recruited. This lowers the overshoot due to early recruitment as seen in Figure 4.7a while improving the tracking performance. The MVS has the best performance for a k_{th} of 0.75. However at lower k_{th} values between 0.6-0.7, there is a significant overshoot in the MVS causing a degradation in performance as seen in Figure 4.7. These trends seem to apply across a range of trajectory frequencies as seen Figure 4.8 where MVS has a performance gains with lower threshold factors with the ideal threshold factor for MVS shifting based on the trajectory frequency. The threshold factor can also impact system efficiency as it alters the amount of time bundle is in different recruitment states, these results are discussed in detail in the following section.

4.4 System with Different Valve Configurations

In addition to tracking accuracy, efficiency of operation is also an important parameter to evaluate the performance of the valve systems. Efficiency of the valve system, η is defined as the ratio of energy output and energy input to the FAM bundle as shown in Equation 4.7. The energy output of the bundle is mechanical work done by the FAMs, W_{bundle} and energy input to the bundle is the fluid energy input, E_{in} . Energy consumption due to fluid compression was considered to be negligible since the operating fluid has very high bulk modulus. This definition of efficiency dictates that the system is the most efficient when the FAMs operate near the supply pressure and its efficiency degrades when the FAMs are

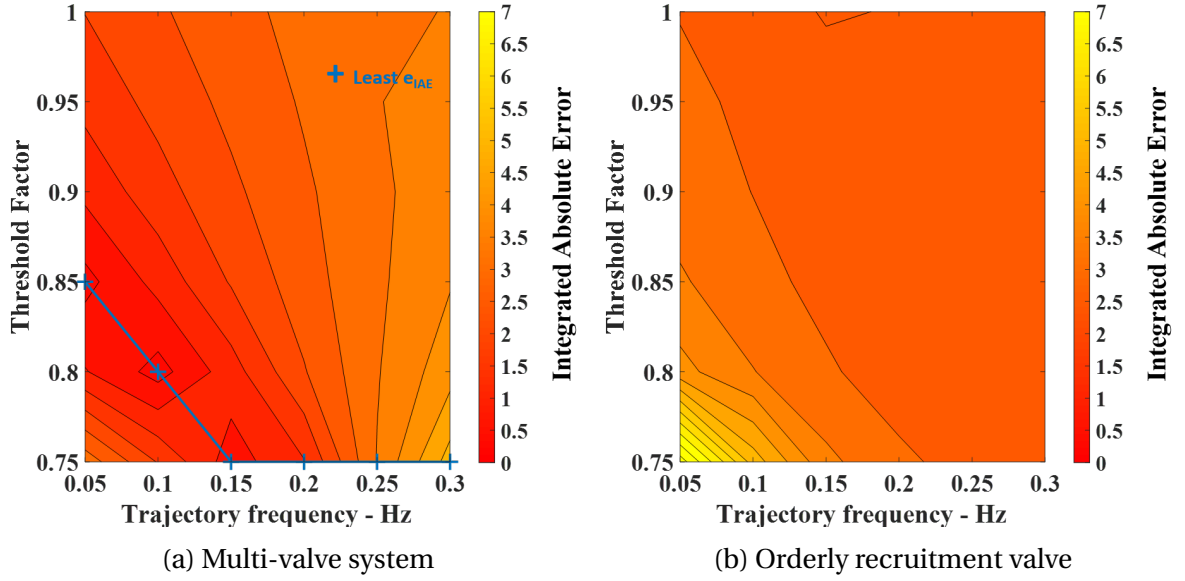


Figure 4.8: Trajectory tracking performance of MVS and ORV over a range of frequencies and threshold factors

operating at lower pressures.

$$\eta = \frac{W_{bundle}}{E_{in}} \quad (4.7)$$

The work done by the actuators in rotating the arm is the total work done by the FAM actuators as shown in Equation 4.8.

$$W_{bundle} = \int F_{m,1} \dot{x}_{m,1} + \int F_{m,2} \dot{x}_{m,2} \quad (4.8)$$

The fluid energy input is the work done by the accumulator to drive the volume change in the FAMs as given in Equation 4.9.

$$E_{in} = \int P_s (\dot{V}_{m,1} + \dot{V}_{m,2}) \quad (4.9)$$

Effects of threshold factor on the efficiency of the system are identified through a series

of trajectory tracking simulations. Trajectories with an arm rotation of 45^0 and frequencies ranging between 0.05 Hz to 0.3 Hz were simulated and presented in the contour plots in Figure 4.9. Figure 4.9a shows that the MVS system is 1.2 times more efficient at higher threshold factors across frequencies which can be attributed to the fact that at lower threshold factor FAM 1 is forced to operate at lower pressures for a longer period of time. Conversely at higher threshold factors, FAM 1 operates at relatively higher pressures that are closer to supply pressure. As shown in Figure 4.9b, threshold factor does not have a significant effect on the efficiency of ORV as FAM 1 saturation is not restricted like it is in the MVS.

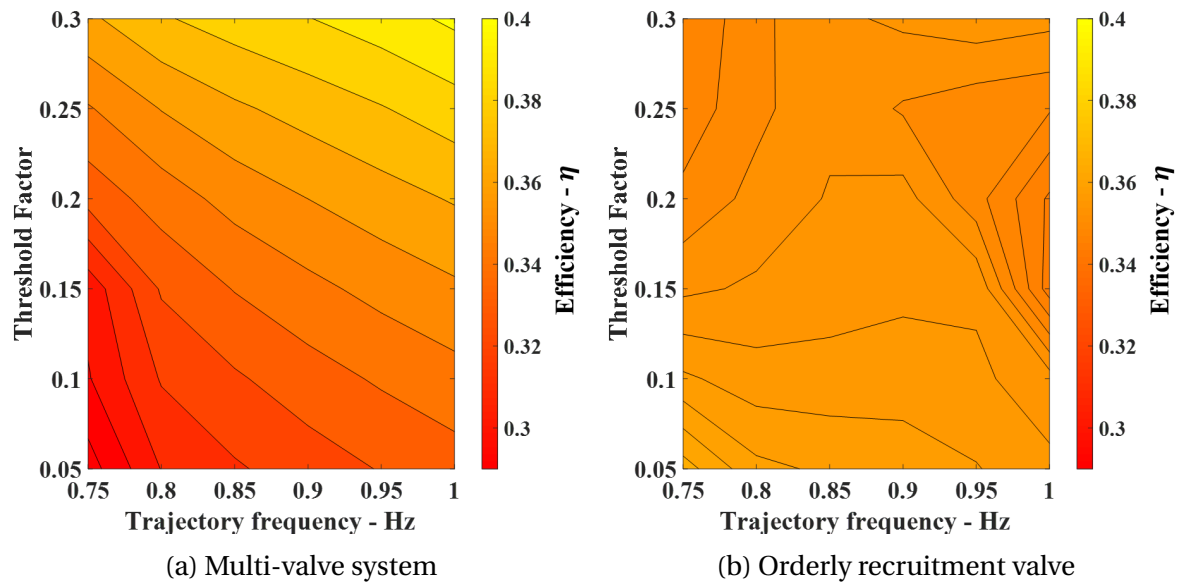


Figure 4.9: Efficiency of MVS and ORV systems over a range of frequencies and threshold factors

Efficiencies of the MVS are between 28.54% and 40.12% with maximum efficiency when tracking a trajectory with a frequency of 0.3 Hz at a threshold factor of 1. For the ORV efficiencies range between 34.5% and 36.49% with maximum efficiency when tracking a trajectory of 0.05 Hz at a threshold factor of 0.75. To summarize, these results show the

trade-off between accuracy and efficiency using the threshold factor in MVS and also show that the ORV is passive to the threshold factor. Also, the ability to tune the behavior of the system using the threshold factor highlights additional control flexibility in MVS due to its independent valve system over the single valve system of the ORV.

CHAPTER

5

CONCLUSIONS

The primary focus of this research is to design and develop a novel orderly recruitment valve (ORV) to implement variable recruitment strategy. The thesis first presents a detailed analytical model of the ORV and its unique design characteristics. To analyze the behavior of the ORV it is simulated in conjunction with a rotating arm plant. Analytical models for all the subsystems in the plant model were developed with sufficient fidelity to capture the different dynamics of the system.

In later sections, focus was placed on the implementation of a bio-inspired orderly recruitment strategy that can sequentially recruit FAM units based on the load. The orderly recruitment strategy was embedded into a model-based feed forward controller. This controller was designed to anticipate the required input while fully considering the dynamics

of the system.

Further, the performance of the ORV system with its feed forward controller was demonstrated through a series of trajectory tracking simulations. These simulations revealed a loss in tracking accuracy during the recruitment phase of the system with a significant dip in the trajectory. The recruitment phase of the system revealed the unique flow and spool dynamics of the ORV. To further benchmark the performance of the ORV it was compared to a conventional multi-valve system (MVS) with equivalent dynamics and controller. Initial comparisons showed that the ORV, due to its distinctive characteristics like the cross-flow, had a lower over all tracking error compared to the MVS.

Research focus was placed on tuning of the orderly recruitment strategy to further improve the accuracy of the system. Threshold factor was introduced as a tuning parameter with which significant improvement in the performance of the MVS was obtained with a sacrifice in efficiency. Although the performance of the ORV was comparable to that of the MVS, the inability to tune the performance of the ORV with the threshold factor highlights the design limitations of the ORV. To conclude, even with its design limitations, the ORV can be still be considered as a potential alternative to the MVS where system simplicity is the priority.

5.1 Future Work

Further research can be carried out in three different directions based on the approach established by this research. Primary focus can be on eliminating or minimizing the performance limitations of the ORV through design modifications or control methodologies. Secondly, the analytical models developed in this research presented a good case study to identify the unique behavior of the ORV and a comparative study. However there is scope for improvement in detail of the analytical models where certain ideal case assumptions

were made. Considering a more realistic analytical model can increase the validity of the simulation work and give us more accurate parameters. Finally, an experimental setup can be developed to validate the performance of the proposed design.

REFERENCES

- [1] Andrikopoulos, G., Nikolakopoulos, G., and Manesis, S. (2011). A survey on applications of pneumatic artificial muscles. In *2011 19th Mediterranean Conference on Control & Automation (MED)*, pages 1439–1446. IEEE.
- [2] Bryant, M., Meller, M. A., and Garcia, E. (2014). Variable recruitment fluidic artificial muscles: modeling and experiments. *Smart Materials and Structures*, 23(7):074009.
- [3] Buchthal, F. and Schmalbruch, H. (1980). Motor unit of mammalian muscle. *Physiological Reviews*, 60(1):90–142.
- [4] Chang, M.-K. (2010). An adaptive self-organizing fuzzy sliding mode controller for a 2-dof rehabilitation robot actuated by pneumatic muscle actuators. *Control Engineering Practice*, 18(1):13–22.
- [5] Chapman, E. M. and Bryant, M. (2018). Bioinspired passive variable recruitment of fluidic artificial muscles. *Journal of Intelligent Material Systems and Structures*, 29(15):3067–3081.
- [6] De Volder, M., Moers, A., and Reynaerts, D. (2011). Fabrication and control of miniature mckibben actuators. *Sensors and Actuators A: Physical*, 166(1):111–116.
- [7] Henneman, E., Somjen, G., and Carpenter, D. O. (1965). Excitability and inhibibility of motoneurons of different sizes. *Journal of neurophysiology*, 28(3):599–620.
- [8] Jelali, M. and Kroll, A. (2012). *Hydraulic servo-systems: modelling, identification and control*. Springer Science & Business Media.
- [9] Jiang, X., Xiong, C., Sun, R., Huang, X., and Xiong, Y. (2011). Static and dynamic characteristics of rehabilitation joint powered by pneumatic muscles. *Industrial Robot: An International Journal*, 38(5):486–491.
- [10] Manring, N. (2005). *Hydraulic Control Systems*. Wiley.
- [11] Meller, M., Chipka, J., Volkov, A., Bryant, M., and Garcia, E. (2016). Improving actuation efficiency through variable recruitment hydraulic mckibben muscles: modeling, orderly recruitment control, and experiments. *Bioinspiration & biomimetics*, 11(6):065004.
- [12] Meller, M., Kogan, B., Bryant, M., and Garcia, E. (2018). Model-based feedforward and cascade control of hydraulic mckibben muscles. *Sensors and Actuators A: Physical*, 275:88–98.
- [13] Meller, M. A., Bryant, M., and Garcia, E. (2014). Reconsidering the mckibben muscle: Energetics, operating fluid, and bladder material. *Journal of Intelligent Material Systems and Structures*, 25(18):2276–2293.

- [MOOG] MOOG. Moog servo valves g761/761 series catalog.
- [15] Mori, M., Suzumori, K., Takahashi, M., and Hosoya, T. (2010). Very high force hydraulic mckibben artificial muscle with a p-phenylene-2, 6-benzobisoxazole cord sleeve. *Advanced Robotics*, 24(1-2):233–254.
- [16] Ramsey, R. W. and Street, S. F. (1940). The isometric length-tension diagram of isolated skeletal muscle fibers of the frog. *Journal of Cellular and Comparative Physiology*, 15(1):11–34.
- [17] Robinson, R. M., Kothera, C. S., and Wereley, N. M. (2015). Quasi-static nonlinear response of pneumatic artificial muscles for both agonistic and antagonistic actuation modes. *Journal of Intelligent Material Systems and Structures*, 26(7):796–809.
- [18] Tiwari, R., Meller, M. A., Wajcs, K. B., Moses, C., Reveles, I., and Garcia, E. (2012). Hydraulic artificial muscles. *Journal of Intelligent Material Systems and Structures*, 23(3):301–312.
- [19] Tondu, B. (2012). Modelling of the mckibben artificial muscle: A review. *Journal of Intelligent Material Systems and Structures*, 23(3):225–253.
- [20] Tondu, B., Ippolito, S., Guiochet, J., and Daidie, A. (2005). A seven-degrees-of-freedom robot-arm driven by pneumatic artificial muscles for humanoid robots. *The International Journal of Robotics Research*, 24(4):257–274.
- [21] Tondu, B. and Lopez, P. (2000). Modeling and control of mckibben artificial muscle robot actuators. *IEEE control systems*, 20(2):15–38.
- [22] Wu, J., Huang, J., Wang, Y., and Xing, K. (2014). Nonlinear disturbance observer-based dynamic surface control for trajectory tracking of pneumatic muscle system. *IEEE Transactions on Control Systems Technology*, 22(2):440–455.
- [23] Xiang, C., Giannaccini, M. E., Theodoridis, T., Hao, L., Nefti-Meziani, S., and Davis, S. (2016). Variable stiffness mckibben muscles with hydraulic and pneumatic operating modes. *Advanced Robotics*, 30(13):889–899.
- [24] Zhang, Z. and Philen, M. (2012). Pressurized artificial muscles. *Journal of Intelligent Material Systems and Structures*, 23(3):255–268.

APPENDIX

APPENDIX

A

ACRONYMS AND VARIABLES

A summary of all variables is documented in Table A.2.

Table A.1: A summary of acronyms used in alphabetical order.

Acronym	Abbreviation
Active Variable Recruitment	AVR
Cross-Flow	cf
Dead Band	db
Multi-Valve System	MVS
Orderly Recruitment Valve	ORV
Fluidic Artificial Muscle	FAM

Table A.2: A summary of common variables in alphabetical order.

Variable	Abbreviation
Accumulator pressure	P_s
Arm angle	θ
Arm angular displacement	θ
Arm mass	m_a
Change in the FAM volume	δV_m
FAM axial force output	F
FAM contractile force	F_{bundle}
FAM contraction	x_m
FAM contraction velocity	\dot{x}_m
FAM recruitment state	RS
FAM reference position	θ_{ref}
FAM threshold factor	k_{th}
FAM volume	V_m
Fluid compressibility	β
FAM pressure	P
Free-strain contraction	x_{free}
Integrated absolute error (IAE)	e_{IAE}
Initial accumulator pressure	P_{si}
Initial accumulator volume	V_{si}
Initial FAM length	l_0
Initial FAM radius	r_0

Initial FAM braid angle	α_0
Maximum stroke of the valve	$x_{v,max}$
Motor back emf constant	k_b
Motor coil inductance	L_m
Motor coil resistance	R_m
Motor current	I_m
Motor supply voltage	V_{motor}
Motor torque constant	K_m
ORV cross-flow	Q_{cf}
ORV dead band	x_{db}
ORV port opening diameter	x_v
ORV spool position	x_v
ORV spool width	x_{sw}
PI control input	u_{pi}
PI trajectory error	e
Pulley mass	m_p
Pulley radius	r_p
Pump angular displacement	θ_p
Pump impeller torque	τ_p
Pump rotational inertia	J_p
Pump volume	V_p
Rate of change of FAM contraction	$\delta \dot{x}_m$
Rate of change of FAM volume	\dot{V}_m
Required FAM force	F_{req}
Required FAM contraction	$x_{m,req}$

Required FAM spool position	$x_{v,req}$
Required valve flow rate	$Q_{m,req}$
Required valve supply pressure	$P_{s,req}$
System damping	c
System moment of inertia	I
Supply pressure	P_s
Tip mass	m
Torque due to external load	τ_{load}
Valve damping coefficient	D_v
Valve feed forward input	u_{ff}
Valve flow coefficient	c_v
Valve gain	K_v
Valve hysteresis	f_{hs}
Valve input signal	u_v
Valve nominal flow	Q_N
Valve nominal pressure drop	Δp_N
Valve natural frequency	ω_v